Atomistic Models of Amorphous Polybutadienes. 2. Poly(1,4-*trans*-butadiene), Poly(1,2-butadiene), and a Random Copolymer of 1,4-*trans*-Butadiene, 1,4-*cis*-Butadiene, and 1,2-Butadiene

Eung-Gun Kim, Sanjay Misra, and Wayne L. Mattice*

Institute of Polymer Science, The University of Akron, Akron, Ohio 44325-3909

Received January 14, 1993; Revised Manuscript Received March 22, 1993

ABSTRACT: Atomistic models of amorphous poly(1,4-*trans*-butadiene) and isotactic poly(1,2-butadiene) have been obtained at bulk density by carrying out molecular mechanics and molecular dynamics calculations under periodic boundary conditions, along the lines of the previous study of poly(1,4-*cis*-butadiene). In addition, a model structure has also been obtained for a random copolymer of the *trans* (55%), *cis* (35%) and vinyl (10%) units. From the equilibrated structures, the cohesive energy and solubility parameter are calculated. The characteristic intermolecular packing is discussed in detail for these amorphous structures in terms of the pair correlation functions, along with that of poly(1,4-*cis*-butadiene), which turns out to be significantly different for all four structures. The calculation of conformational statistics of the pure *trans* structure reveals that it retains the properties predicted by the rotational isomeric state (RIS) theory. Also provided here are the results of conformational analysis on the vinyl structure, for which no thorough RIS analysis has been done. The conformational analysis of the mixed structure shows no significant deviation from the results obtained for the pure *trans*, *cis*, or vinyl structures.

1. Introduction

Models for polymeric systems that are realistic at atomic scales can provide detailed information which can aid the materials scientist in the suitable design of materials or experiments, or rationalize macroscopically observed behavior from a microscopic standpoint. Atomistic computer simulations of *amorphous* polymers have gained a tremendous impetus from the work of Theodorou and Suter.[1] In their pioneering work, they devised an energy minimization scheme leading to equilibrium conformations for amorphous atactic polypropylene. These equilibrium structures were then analyzed to deduce the properties of the amorphous polypropylene, thermodynamic and mechanical. Atomistic models of amorphous polymers have seen various improvements since then.[2-5] Two of the more important ones are increasingly detailed and improved force fields for interatomic interactions and more elaborate minimization schemes.

Recently, our group reported results on the atomistic modeling of amorphous poly(1,4-*cis*-butadiene) (*cis*-PBD).[6] In the present work, we have extended our study to the amorphous structures of poly(1,4-*trans*-butadiene) (*trans*-PBD), isotactic poly(1,2-butadiene) (vinyl-PBD), and a random copolymer of *trans* (55%), *cis* (35%), and vinyl (10%) units (mixed-PBD). There have been comprehensive studies[7-9] done on *trans*- and *cis*-PBD single chains based upon the rotational isomeric state (RIS) theory. Later, a series of papers[10-14] were published, presenting results of conformational and packing energy calculations on four polymers of *trans*-, *cis*-, and isotactic and syndiotactic vinyl-PBDs. Unlike *trans*- or *cis*-PBD, no RIS analysis has been reported on vinyl-PBD. Even though they[11-13] provided potential energy maps for isolated vinyl-PBD chains, they did not carry out detailed conformational analysis of the chain; that is, they only used the energy maps to locate a conformation of minimum energy from which various unit cells (crystalline) were produced to carry out packing energy calculations.

The amorphous structures in the present work were analyzed with a view to extracting the following information. Of specific interest were (i) cohesive energy and the Hildebrand solubility parameter, (ii) intermolecular packing, and (iii) conformations of PBD chains in the amorphous bulk.

2. Computational Details

The molecular mechanics and molecular dynamics calculations for this work were carried out by using POLYGRAF 2.20.[15] The overall potential of the system, E, was calculated as

$$E = E_{\text{stretching}} + E_{\text{bending}} + E_{\text{torsion}} + E_{\text{oop}} + E_{\text{vdW}} \qquad (1)$$

The out-of-plane energy E_{oop} applies only to planar groups containing an sp^2 central atom bonded to three other atoms, and is given as $E_{\text{oop}} = K_\omega(1 - \cos\omega)$ where ω is the angle between one bond and the plane formed by the other two, and K_ω the force constant. All the individual hydrogen atoms were taken into account in our calculations. Parameters of the Dreiding force field were modified for the present study, which proved successful for modeling polybutadienes.[6,16-18]

The parent chain comprising 99 monomeric units (992 atoms) was packed into the cubic simulation box at a density of 0.89 g/cm^3 (corresponds to room temperature)[19] under periodic boundary conditions via Monte Carlo methods. Generation of the initial dihedral angles depends on the pairwise sum of the atomic radii (reduced to 30% of the full van der Waals radii). If the nonbonded distance of two atoms is smaller than the sum of their atomic radii, that conformation is rejected in the growing process. The algorithm will try other dihedral angles in a random fashion until an allowed distance can be obtained. If necessary, bonds previously assigned near the growing end will be erased and placed anew. No rotational energy barrier is taken into account during the growing process. The parent chain of mixed-PBD contained 54 *trans*, 35 *cis*, and 10 vinyl units randomly distributed along the chain. The resulting box edge length was 21.541 Å. This poorly packed initial structure was relaxed by the strategy developed recently in our group.[6,20] The relaxation strategy used is as follows: (1) Minimize the potential energy of the initial structure using the conjugate gradient method. (2) Heat up the structure obtained in step 1 from 0 K to a very high temperature of 1000 K and run a short molecular dynamics trajectory at 1000 K. (3) Extract a conformer of the lowest total potential energy from the later stage of the "high temperature dynamics" trajectory, and minimize the potential energy of the extracted structure as done in step 1. The overall time duration in step 2 is 5–10 ps, and the heating rate is 100 K/0.1 ps. All the calculations are carried out at a constant volume, which is

0024-9297/93/2226-3424$04.00/0

Table I. Values of E_{coh} and δ for *trans*-, *cis*-, Vinyl-, and Mixed-PBDs

polymer	E_{coh} (cal/mol)	δ (cal$^{1/2}$/cm$^{3/2}$)
trans	3982 ● 441	8.09 ± 0.45
cis[6]	4100 ● 350	8.23 ± 0.70
vinyl	2998 ± 327	7.02 ● 0.38
mixed	4000 ± 150	8.11 ± 0.30
experiment[19]	3980–4490	8.1–8.6

Table II. Total Potential Energy Decompositions (kcal/mol of chains) for Five Structures of Mixed-PBD

structure no.	total	stretching	bending	torsion	oop	vdW
1	557.03	91.36	219.95	169.28	2.45	73.99
2	563.33	91.25	201.08	198.82	2.64	69.55
3	562.82	88.68	212.87	182.75	2.49	76.03
4	569.59	89.32	201.43	190.15	2.73	85.95
5	568.79	91.49	214.73	188.40	1.79	72.38
s_x	5.10	1.32	8.41	10.92	0.37	6.26

important especially during the molecular dynamics calculations in order to keep our system stable at such an unrealistically high temperature.[6] The overall potential energy of the equilibrated amorphous cells after step 3 was lower by 15–25% than that after the energy minimization in step 1. Five structures for each type of polybutadiene were independently generated and equilibrated according to the procedures described above. All the results presented here are the ensemble averages of the five structures.

3. Results and Discussion

3.1. Cohesive Energy and the Hildebrand Solubility Parameter. The cohesive energy E_{coh} is defined[19] as the increase in internal energy per mole of substance if all intermolecular forces are eliminated. E_{coh} can thus be estimated as the ensemble average of the difference[1]

$$E_{coh} = E_{isolated} - E_{bulk} \quad (2)$$

The Hildebrand solubility parameter δ is then defined as follows:

$$\delta = (E_{coh}/V)^{1/2} \quad (3)$$

where V is the volume of 1 mol of monomeric units. The values of E_{coh} and δ for *trans*-, vinyl-, and mixed-PBDs and for *cis*-PBD[6] are listed in Table I. Table II shows values of each component of the total potential energy for mixed-PBD, where each value is given for 1 mol of parent chains.

It is worthwhile to make a comparison of the cohesive energy (or Hildebrand solubility parameter) obtained from our model structures with that from experiments. An agreement between the calculated and experimental values is observed for *trans*- and mixed-PBDs as for *cis*-PBD.[6] Calculated values for vinyl-PBD, however, are significantly lower than the experimental ones. Since the experimental value[19] given in Table I is obtained for a polybutadiene mixture composed mostly of *trans* and *cis* units (55/35/10 *trans*/*cis*/vinyl), it is not unexpected that the results for the pure *trans* and *cis* structures are in good agreement with experiments. Also it is not surprising that our pure vinyl structure has a δ different from that of a polymer for which the vinyl content is only 10%.

From the definition of the cohesive energy used for the calculation, eq 2, the cohesive energy is the difference in the van der Waals interaction energy term between the isolated and bulk chain. The values of the van der Waals interaction energy term for the structures are given in Table III. For vinyl-PBD, the van der Waals component

Table III. Calculated Values of the van der Waals Interaction Energy, E_{vdW} (kcal/mol of chains), for *trans*-, *cis*-, Vinyl-, and Mixed-PBDs

polymer	E_{vdW}(isolated)	E_{vdW}(bulk)
trans	459.48 ± 41.06	65.26 ± 8.04
cis[6]	461	54.55
vinyl	499.45 ± 26.49	202.63 ± 8.34
mixed	470.51 ± 22.91	75.58 ± 6.26

of about 500 kcal/mol for the isolated chain decreases to about 200 kcal/mol for the parent chain in the bulk. For the *trans*, *cis*, or mixed structure, on the contrary, the van der Waals contribution drops from about 460 to about 60 kcal/mol. In other words, the intramolecular van der Waals contribution is about the same for all four structures, but is largely diminished by the intermolecular van der Waals contribution for the *trans*, *cis*, or mixed structure. The only way for the parent chain to effectively diminish the large, positive intramolecular van der Waals interactions is, in principle, to find atoms from the neighboring chains that can "solvate" every atom of the parent chain at a distance at which the van der Waals interaction energy becomes the lowest (largest negative value). The bulky side groups of the vinyl-PBD chain make it difficult for the solvating atoms to access the backbone atoms of the parent chain while the absence of side chains in the *trans*- and *cis*-PBD chains (and also in most parts of the mixed-PBD chain) allows an easier solvation. However, this does not necessitate a loose packing, or a decrease in density of the vinyl structure because the backbone carbon atoms are surrounded well by the bulky side groups (further molecular mechanical energy minimization of the vinyl structures with cell parameters optimized during calculation showed only a 3% increase in volume and a 3% decrease in δ). This argument is manifested in the intermolecular radial distribution functions for the carbon-carbon pair, which will be discussed in detail in the following section.

It is also worthwhile to note that interactions between neighboring vinyl side groups do not lower the intramolecular van der Waals energy of vinyl-PBD from its isomers (Table III). This will also be clearly explained when we discuss chain conformations of vinyl-PBD.

3.2. Pair Correlation Functions. Pair correlation (or radial distribution) functions (RDFs) were calculated for various pairs of atoms for three types of contributions: total, intramolecular, and intermolecular. RDFs provide a close quantitative look at how the atoms pack in an amorphous structure. The intramolecular contribution is taken from atom pairs of a parent chain which are in the same amorphous cell. The intermolecular contribution is taken from atom pairs of the parent chain which are not in the same cell.

Figure 1 shows the total RDFs for mixed-PBD. The sharp peaks observed in the total RDFs are the intramolecular contributions. No order beyond 7 Å was observed for all three structures from total RDFs for C/C, H/H, and C/H atom pairs, where no differentiation was made between C_{sp^2} and C_{sp^3}.

Figure 2 shows the intermolecular RDFs of the C/C pair for *trans*-, vinyl-, and mixed-PBDs. For *trans*- and mixed-PBDs, the intermolecular RDF shows a broad peak near 5 Å and a shallow minimum around 7 Å, and rises thereafter to its asymptotic value of unity. A similar behavior was also observed in *cis*-PBD.[6] In contrast, the intermolecular RDF rises monotonically to its asymptotic value in vinyl-PBD.

Decomposition of these intermolecular RDFs of the C/C pair into C_{sp^2}/C_{sp^2}, C_{sp^3}/C_{sp^3}, and C_{sp^2}/C_{sp^3} pair contributions

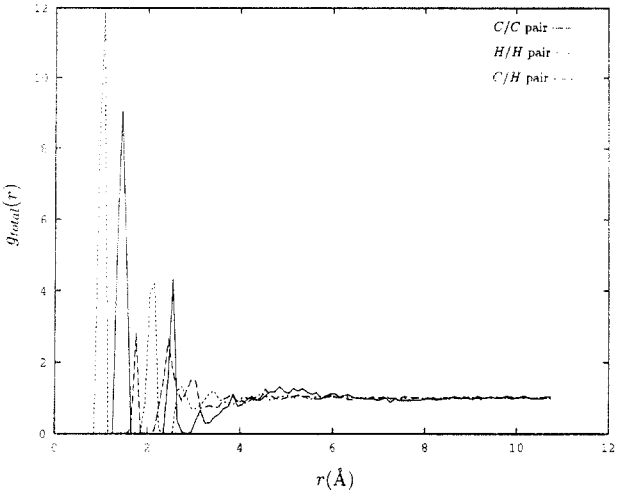

Figure 1. Total RDFs for mixed-PBD.

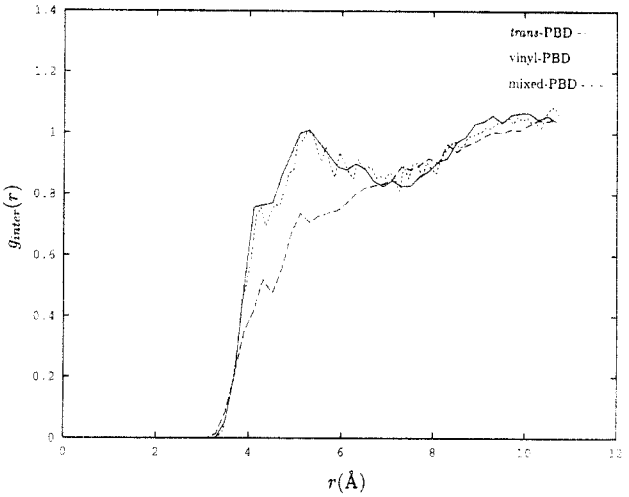

Figure 2. Intermolecular RDFs of the C/C pair for *trans*-, vinyl-, and mixed-PBDs.

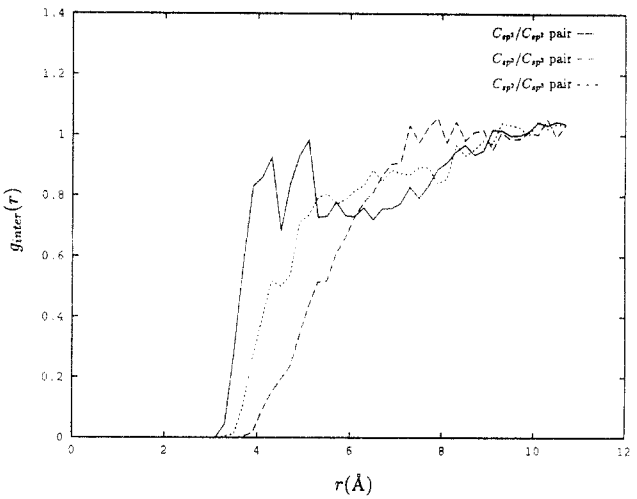

Figure 3. Intermolecular RDFs for vinyl-PBD.

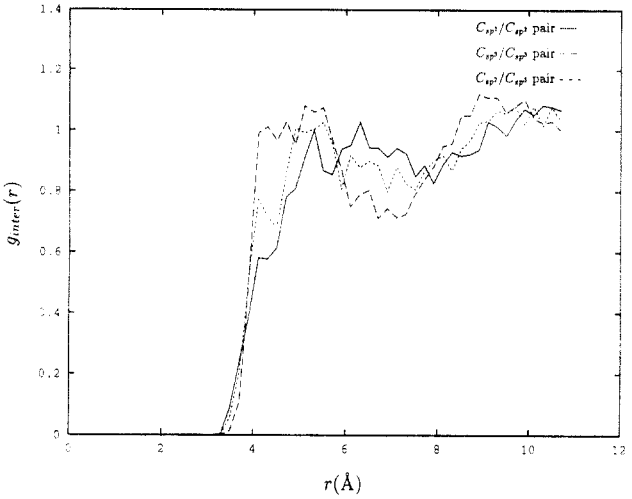

Figure 4. Intermolecular RDFs for *trans*-PBD.

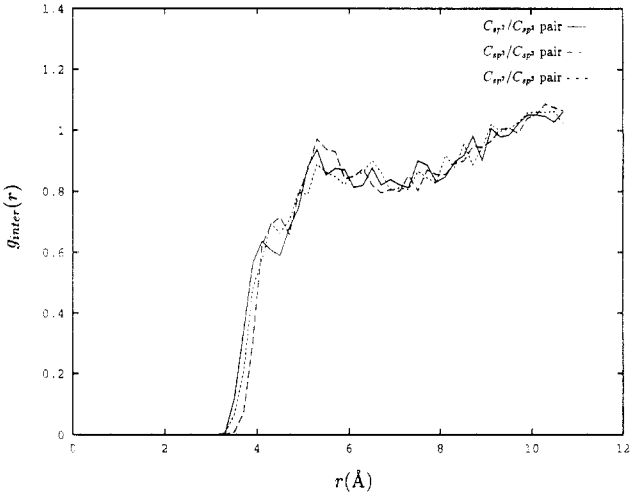

Figure 5. Intermolecular RDFs for *cis*-PBD.

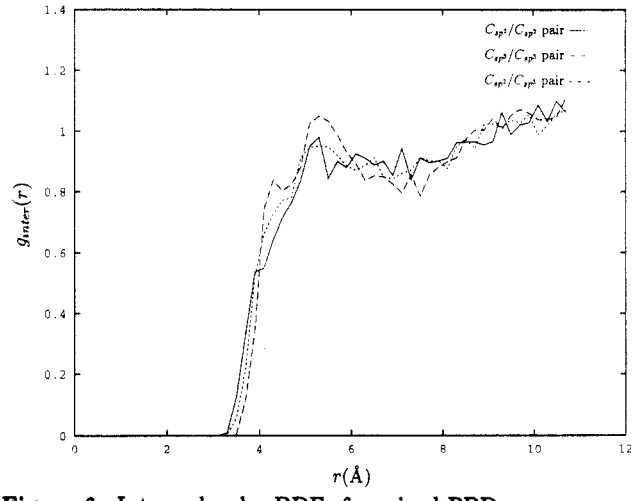

Figure 6. Intermolecular RDFs for mixed-PBD.

makes clearer the differences in intermolecular packing between the four different structures (we also provide here decomposed intermolecular RDFs for *cis*-PBD). The decomposed intermolecular RDFs are given in Figures 3–6. We will discuss first the pure microstructures (*trans*, *cis*, and vinyl) since these can be rationalized unambiguously on the basis of the identical chemical structure of the monomeric units in each of them.

Vinyl-PBD is the easiest case to analyze, for which two peaks are identified in the range of 3.8–5.3 Å in the decomposed intermolecular RDFs (Figure 3), corresponding to the shorter and longer distances between a pair of C_{sp^2} atoms from two closely packed vinyl side groups, as shown in Figure 7. This type of spatial arrangement is possible because vinyl groups are planar and because those bulky side groups of a chain are exposed to the surroundings so as to be accessible by side groups from the other chains. The very small population of C_{sp^3}/C_{sp^3} pairs in the same range can be explained in the same context. The neighbors of backbone C_{sp^3} atoms of a chain are so crowded by the chain's own bulky side groups that the backbone

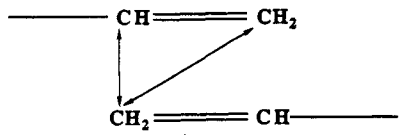

Figure 7. Intermolecular arrangement of two neighboring vinyl side groups.

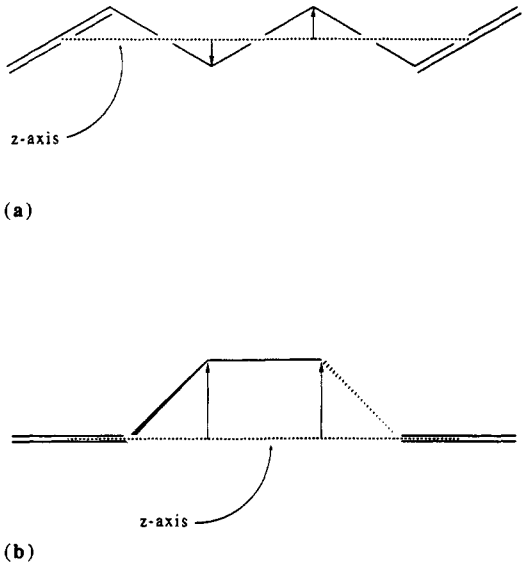

Figure 8. Definition of the protrusion distance for the C_{sp^3} atom: (a) CH_2–CH_2 in *trans* and (b) CH_2–CH_2 in *gauche*.

carbon atoms of the other chains, also surrounded by their own side groups, can hardly access them.

trans-PBD shows a peak in the population for the C_{sp^3}/C_{sp^3} pair from 4 to 6 Å, and this peak is absent for the C_{sp^2}/C_{sp^2} pair (Figure 4). In the case of *cis*-PBD, on the other hand, one cannot distinguish the decomposed RDFs for the C_{sp^2}/C_{sp^2}, C_{sp^2}/C_{sp^3}, and C_{sp^3}/C_{sp^3} pairs from the combined RDF for all carbon pairs of Li and Mattice[6] (see Figure 5).

The intermolecular arrangement in *trans*- and *cis*-PBDs can be clarified by defining a variable that quantifies the degree of exposure of a particular type of atom to the surroundings. Let us consider all the possible CH=CH—CH_2—CH_2—CH=CH segments in *trans*- and *cis*-PBDs, and imagine a "*z*" axis from the middle of one CH=CH bond to the middle of the next as shown in Figure 8. Calculation of the distance of the C_{sp^3} atom from this *z* axis, defined here as the *protrusion distance* of the C_{sp^3} atom, tells us the extent of exposure to the surroundings of the C_{sp^3} atoms from the "imaginary" chain backbone formed by those *z* axes. The same calculation also can be carried out for the C_{sp^2} atom, whose *z* axis is now defined by the middle of one CH_2—CH_2 bond and the middle of the next in each CH_2—CH_2—CH=CH—CH_2—CH_2 segment, as shown in Figure 9. The distributions of the protrusion distance are given in Figures 10 and 11, where the solid curves are for the C_{sp^3} atoms and the dashed ones for the C_{sp^2} atoms. The double peaks in Figures 10 and 11 indicate that the extent of protrusion of the C_{sp^3} atom along the imaginary chain is essentially the same for both *trans*- and *cis*-PBD. It is apparent from Figure 8 that the first (at a shorter protrusion distance) and second (at a longer protrusion distance) peaks of the double peaks take the contributions from the *trans* states and from the *gauche* states, respectively, assumed by the CH_2—CH_2 bonds. It is also expected to observe only a single peak for the C_{sp^2} atom in *trans*- or *cis*-PBD from the fact that the CH=CH bond can only assume a single conformational state in a given microstructure (see Figure 9). Figure 10

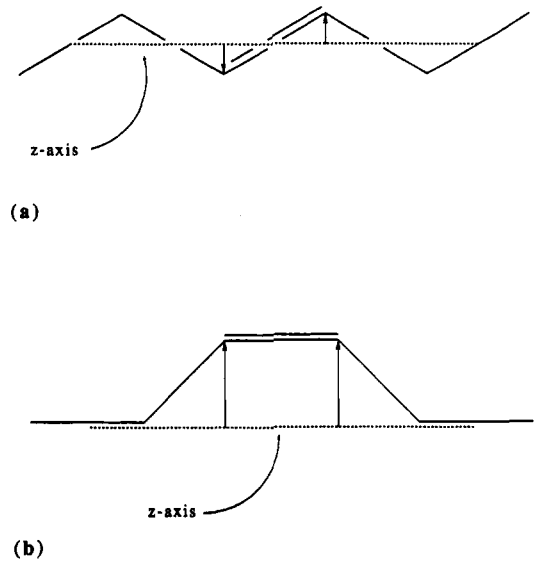

Figure 9. Definition of the protrusion distance for the C_{sp^2} atom: (a) CH=CH in *trans* and (b) CH=CH in *cis*.

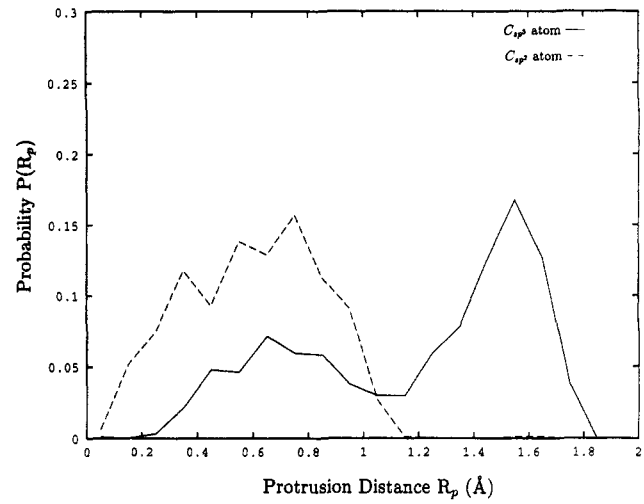

Figure 10. Distributions of the protrusion distance of the C_{sp^3} and C_{sp^2} atoms for *trans*-PBD.

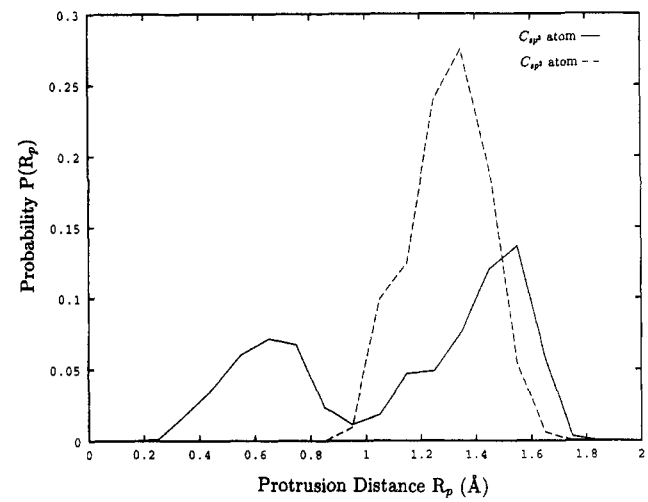

Figure 11. Distributions of the protrusion distance of the C_{sp^3} and C_{sp^2} atoms for *cis*-PBD.

indicates about two thirds of all C_{sp^3} atoms of a *trans*-PBD chain assume larger protrusion distances than most of the C_{sp^2} atoms. In a *cis*-PBD chain, on the other hand, most of the C_{sp^2} atoms and two thirds of the C_{sp^3} atoms are found in the same range of protrusion distance, as shown in Figure 11.

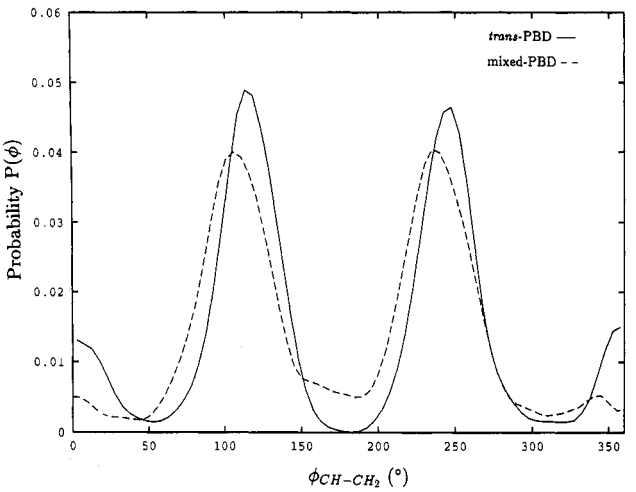

Figure 12. Distributions of dihedral angles for the CH–CH_2 bond in *trans*- and mixed-PBDs.

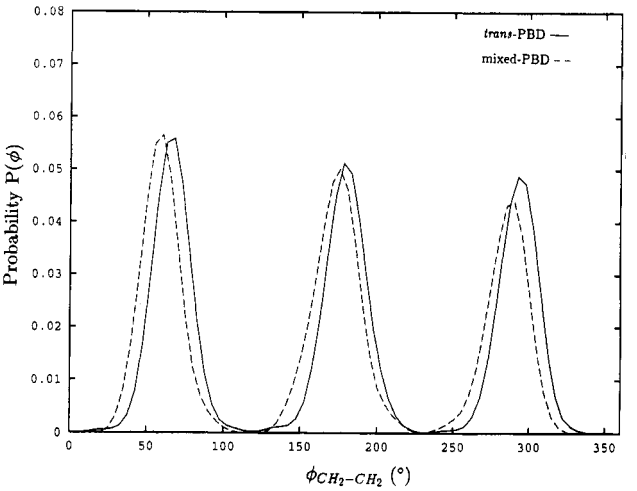

Figure 13. Distributions of dihedral angles for the CH_2–CH_2 bond in *trans*- and mixed-PBDs.

With this new information in hand, we revisit the intermolecular RDFs for the *trans* and *cis* structures. The analysis is now straightforward by using the same argument as we adopted in explaining the intermolecular RDFs for vinyl-PBD. For *trans*-PBD, the C_{sp^3} atoms, mostly from the CH_2–CH_2 segments in *gauche* states, are more exposed to the surroundings than the C_{sp^2} atoms, and therefore more likely to be solvated by the same species of the other chains, leading to the strong peak appearing in the range of 4–6 Å in the RDF for the C_{sp^3}/C_{sp^3} pair. For *cis*-PBD, on the other hand, both the C_{sp^3} atoms of the CH_2–CH_2 segments in *gauche* states and the C_{sp^2} atoms are exposed to the same extent, giving rise to peaks at the same location in the intermolecular RDFs for the C_{sp^3}/C_{sp^3} and C_{sp^2}/C_{sp^2} pairs. Since the equal protrusion of the C_{sp^2} atoms limits access to the C_{sp^3} atoms and vice versa, the peak intensity of the RDFs for both pairs in *cis*-PBD is weak compared to that for the C_{sp^3}/C_{sp^3} pair in *trans*-PBD.

Turning to the intermolecular RDFs for mixed-PBD, we benefit from insights into *trans*- and *cis*-PBDs. The intermolecular RDFs for decomposed carbon pairs are closer to those for *cis*-PBD although *cis* units constitute only 35% of the structure (see Figures 5 and 6). Although the situation may be expected to be dominated by the *trans* units, there is no evidence of the strong peak in the RDF of the C_{sp^3}/C_{sp^3} pair. Its absence is attributed to the lower concentration of *trans* units and the random placement of the *trans* and *cis* units, which rob C_{sp^3} atoms of any preferential protrusion.

3.3. Chain Conformations. 3.3.1. *trans*-PBD. The solid curves in Figures 12 and 13 show the overall distributions of rotational states of CH–CH_2 and CH_2–CH_2 bonds for the amorphous *trans*-PBD chain. In Figure 12, one can identify peaks at 180 ± 60° corresponding to *anticlinal*$^+$ (A^+) and *anticlinal*$^-$ (A^-), respectively, and also a rather small peak at 0° or *cis* which is not observed in *cis*-PBD because of the severe steric overlaps between $(CH_2)^0$ and $(CH_2)^4$ [6,7,9] (see Figure 14a). The relatively small population at *cis*, in contrast to the calculations of Mark[8] and Abe and Flory,[9] is due to the larger value[6,14,16] adopted in our calculations for the energy difference between *cis* and *anticlinal*$^\pm$ in order to take into account the slight steric overlaps between hydrogen atoms, $(H)^0$ and a pair of $(H)^3$s in Figure 14b. One can also notice the disappearance of the small population in the *trans* domain that occurs in the *cis* structure to alleviate steric overlaps between pairs of methylenic hydrogens.[6,7,9]

In Figure 13, all three rotational states, *trans* (T) and *gauche*$^\pm$ ($G^\pm$), of the CH_2–CH_2 bond seem to be almost equally populated. The RIS analysis[7,8] showed that the first-order interaction between methine groups is much smaller than that between methylene groups in a polyethylene chain, and that the statistical weight of *gauche* states approximates that of a *trans* state. The RIS calculations[8,9] also show, on the other hand, that the *gauche* states become less probable when the adjoining CH–CH_2 bond is in the *cis* conformation in which a second-order interaction occurs between two methine groups, $(CH)^0$ and $(CH)^4$, in Figure 14b. For our *trans* structure, however, the rotational states of CH_2–CH_2 seem to be little perturbed by its adjoining CH–CH_2 bonds because of the relatively small population at *cis* of the CH–CH_2 bonds.

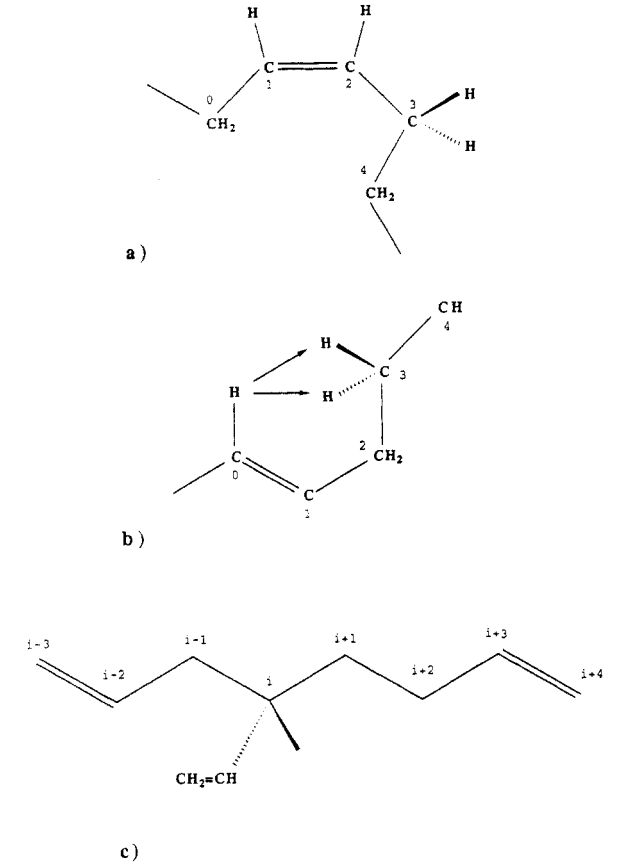

Figure 14. Structures of (a) *cis*-, (b) *trans*-, and (c) mixed-PBDs.

Figures 15 and 16 show the correlated distributions of dihedral angles for neighboring CH—CH_2/CH_2—CH_2

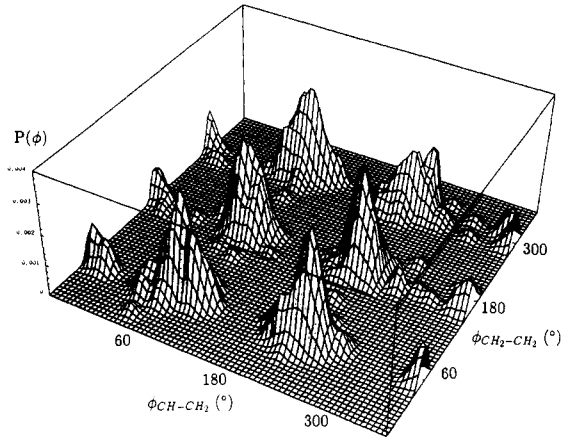

Figure 15. Correlated distribution of dihedral angles for the CH–CH_2/CH_2–CH_2 bond pair in *trans*-PBD.

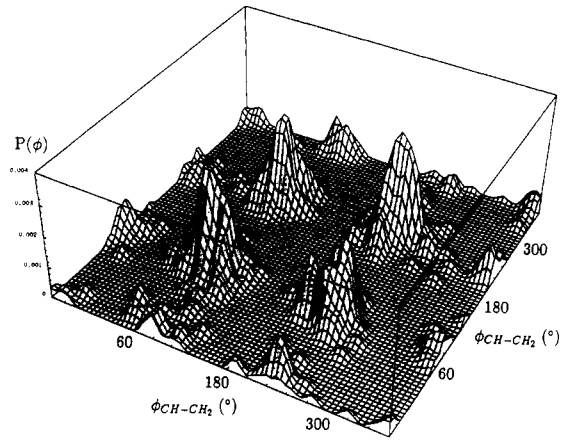

Figure 16. Correlated distribution of dihedral angles for the CH–CH_2/CH_2–CH bond pair between two consecutive double bonds in *trans*-PBD.

bond pairs and for CH—CH_2/CH_2—CH bond pairs between two consecutive double bonds. The three rotational states T and $G^{\pm}$ for the CH_2—CH_2 bond are almost equally populated regardless of the conformations assumed by the adjoining CH—CH_2 bonds (Figure 15). From the results of previous conformational energy calculations by De Rosa et al.,[14] it is easy to expect four dominant peaks at $A^{\pm}A^{\pm}$ and $A^{\pm}A^{\mp}$ for two CH—CH_2 bonds separated by CH=CH or CH_2—CH_2 (Figure 16). The $A^{\pm}A^{\pm}$ pairs are slighly preferable to the $A^{\pm}A^{\mp}$ pairs.[14,16] And also, small peaks of about the same magnitude are observed at every pair of rotational states that has one or two *cis* states.

3.3.2. Vinyl-PBD. The solid curve in Figure 17 shows the overall distribution of rotational states ϕ of skeletal bonds of the isotactic vinyl-PBD chain in the bulk, where the three rotational state domains are well defined. Peak maxima occur at 62.5°, 177.5°, and 297.5°, around which each domain is almost symmetric.

The solid curve in Figure 18 shows the distribution of the torsional rotation χ of the bond connecting a vinyl side group to its α carbon atom. The dihedral angle χ is defined as the angle formed by the double bond of the vinyl side group with respect to the preceding skeletal bond flanking the α carbon, as shown in Figure 19. One can identify in Figure 18 two characteristic regions for χ: one ranging from 30° to 160° and the other from 190° to 300°. We will denote the first domain as *vertical*$^-$ and the second as *vertical*$^+$. This observation naturally raises a question: How are the rotational states in the vicinity of 60° accessible by a C_{sp^2}–C_{sp^3} bond that has inherent local potential minima only at 0° and ±120°? There has been

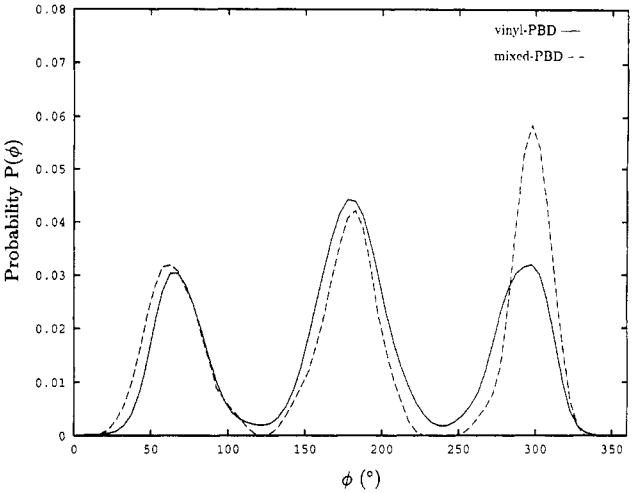

Figure 17. Distributions of dihedral angles for the CH_2—CH-(CH=CH_2)—CH_2 skeletal bonds in vinyl- and mixed-PBDs.

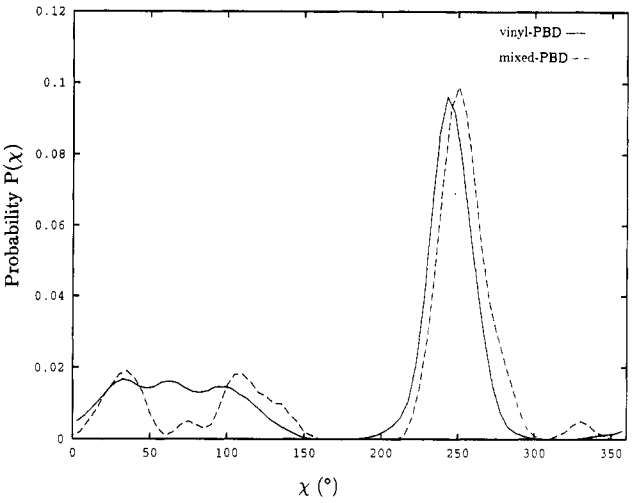

Figure 18. Distributions of dihedral angles χ for the side groups in vinyl- and mixed-PBDs.

one publication by Corradini et al.[12] on conformational energy calculations of an isolated chain of isotactic vinyl-PBD, where they used the results to study the crystalline states of the polymer and, unfortunately, mentioned little about conformations of the vinyl group.

In order to investigate conformational states of side groups, potential energy calculations have been carried out about the C_{sp^2}–C_{sp^3} bond for 3-methyl-1-butene and 3-ethyl-1-pentene (see Figure 20) using the same force field as used for the bulk state of PBDs. In each conformational domain, the energy was minimized with respect to all bond angles, bond lengths, and torsion angles. The results of the calculations are plotted in Figure 21. The calculation on the 3-methyl-1-butene molecule shows that the C_{sp^2}–C_{sp^3} bond has another local energy minimum in addition to those three states available to the C_{sp^2}–C_{sp^3} bond of 1-butene. This local minimum near 60° is only 0.5 kcal/mol higher in energy than the *cis* states (χ = 10° and 110° in Figure 21).

The potential energy calculation on the 3-ethyl-1-pentene molecule was carried out by keeping bond 2 and bond 3 (see Figure 20b) in the domains of T and G^+, respectively. The energy at χ = 65° remains the same (2.75 kcal/mol) relative to that of the *vertical*$^+$ state as before substitution of two methyl groups into 3-methyl-1-butene. The rotational states at 10° and 110° become less favorable than at 65°, even one of which is no longer a local minimum.

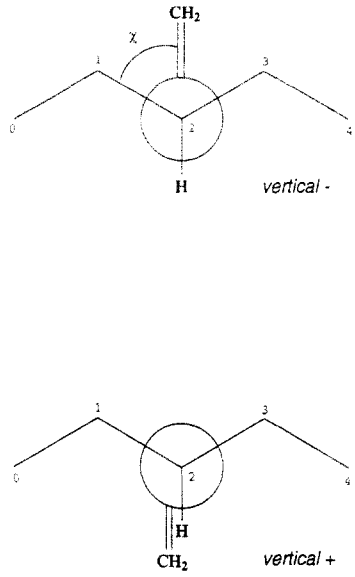

Figure 19. Newman projections of a vinyl-PBD segment.

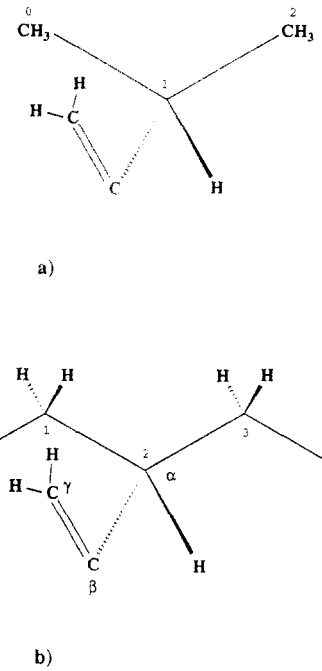

Figure 20. Structures of (a) 3-methyl-1-butene and (b) 3-ethyl-1-pentene.

The above energy calculations suggest that the three states $\chi = 65°$, 10°, and 110° are accessible to one another without gaining an appreciable torsion energy in the absence of any long-range-order interactions with neighboring vinyl side groups occurring in a polymer chain. This is manifested in the triplet of Figure 18.

The rotational state of *vertical*$^+$ is influenced little by the rotational states of the skeletal bonds because the $(CH_2)^\gamma$ group does not participate in any appreciable second, or higher, order interactions in any conformations, which is also well manifested in the narrow distribution of χ around 245° in Figure 18.

Figure 22 shows the correlated distribution of rotational states of the meso diad (*ll* pair used for calculations) for the parent chain in the bulk. One observes five major peaks, all of which are expected from the energy map of

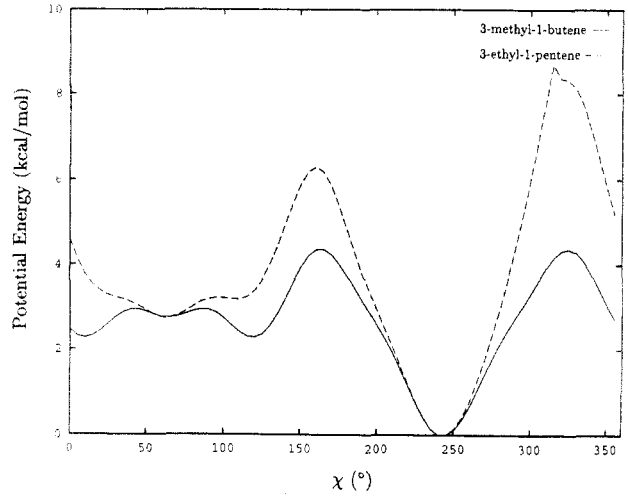

Figure 21. Conformational energy maps for dihedral angles χ in 3-methyl-1-butene and 3-ethyl-1-pentene.

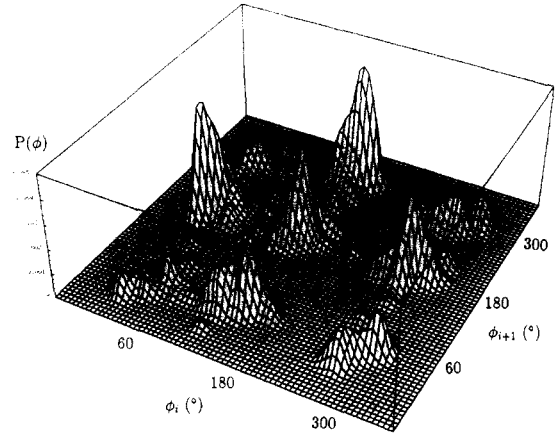

Figure 22. Correlated distribution of dihedral angles for the meso diads in vinyl-PBD.

Corradini et al.[12] Two of the peaks, one in the TG$^+$ domain and the other in the G$^-$T domain, typical of isotactic vinyl polymers,[22] are the most preferred diad conformations. Corradini et al. also observed the existence of TT, 1.8 kcal/mol higher in energy than TG$^+$ or G$^-$T, which they regarded as a consequence of planarity of the side group.[12] The other two peaks at TG$^-$ and G$^+$T, 2.4 kcal/mol higher than TG$^+$ or G$^-$T according to their calculations, also show a strong intensity comparable to that of TT. These significant populations in the domains of TT, TG$^-$, and G$^+$T are attributed to intermolecular interactions which were not taken into account in their energy calculations.

We now revisit the observation in our early discussion that side group–side group interactions do not lower the intramolecular van der Waals energy of vinyl-PBD from those of the other three structures (Table III). Interactions (attractive or repulsive) between neighboring side groups in isotactic vinyl-PBD are not as significant as those in isotactic polystyrene (PS),[21] which was also reported by Corradini et al.[12] This can be understood as follows from the consideration of chemical structures of the side groups in vinyl-PBD and PS. Let's consider a meso diad in the TT state. The number of interacting carbon atoms in each vinyl group is only two, compared to six in the phenyl group of PS. In addition, since a vinyl group can assume either of the two *vertical* states, a diad of opposite *vertical* states leaves only one interacting carbon atom in each vinyl group, which is not the case in PS.

3.3.3. Mixed-PBD. The mixed structure contains all the bond types discussed for *trans*-, *cis*-,[6] and vinyl-PBDs.

Naturally, it is instructive to categorize the bonds and bond pairs in the mixed-PBD chain along the lines of those discussed for the "pure" cases. We specifically consider the $CH–CH_2$ and $CH_2–CH_2$ bonds formed by the *trans* and *cis* units. We also look at the skeletal bonds in the vinyl units and the bond connecting the vinyl side group. Thus separated, the number of bonds of each type, especially the vinyl kind, available for analysis is smaller than in the pure cases. The statistics are correspondingly of larger uncertainty, especially for the vinyl group.

For the purpose of better illustration, the distributions of the rotational states are shown along with corresponding distributions in the pure states. The rotational states of the $CH–CH_2$ and $CH_2–CH_2$ bonds involved in the *trans* and *cis* units are shown as dashed curves in Figures 12 and 13, respectively. The distribution for the $CH–CH_2$ bond shows two characteristic locations, one at *cis* which occurs only in *trans*-PBD and the other at *trans* which occurs only in *cis*-PBD. Indeed, no sigificant difference is obvious, leading to the conclusion that the presence of different neighboring units does not appreciably affect the rotational states of these bonds.

As for the rotational states of the skeletal bond of the vinyl units (dashed curve in Figure 17), one must recognize the skeletal bonds of vinyl units in mixed- and vinyl-PBDs are in two totally different environments. The rotational states of a vinyl polymer are strongly dependent upon both the presence of a side group of the neighboring unit and its tacticity. In this figure, an asymmetry of the *gauche* states is observed, which is due to the fact that the parent chain was grown with the vinyl units scattered along the chain as "isotactic" and the head-to-tail ratio as unity. From this fact, we can easily find an explanation for the preference of G^+ to G^-. It is apparent from Figure 14c that bonds i and $i + 1$ are no longer equivalent. Therefore, $G^\pm$ at bond i is not equivalent to $G^\mp$ at bond $i + 1$. The first-order interactions of chain atoms around bond i in G^+ occur between the methine and methylene groups, and the second-order interactions between groups $i - 3$ and $i + 1$ through $A^\pm G^+$ diad conformations where the sign of *anticlinal* affects little the conformation of bond i. In contrast, the counterpart bond $i + 1$ in G^- undergoes the first-order interactions between methylene groups in the main chain, and the second-order interactions between groups $i - 1$ and $i + 3$ (if one were to imagine formulating the interactions for the chain viewed from right to left, instead of left to right).

Turning to the distribution of the rotational states χ of the bond connecting the side group (dashed curve in Figure 18), we again notice the two domains observed for vinyl-PBD. Notice that the rotational state at 65° is much less favorable than at 10° and 110°, unlike vinyl-PBD. This significantly reduced intensity near 65° is attributed to the absence of vinyl meso diads in the mixed structure due to the small amount of the vinyl units.

Acknowledgment. This work was supported by grants from the Edison Polymer Innovation Corp. (EPIC) and by ARO 03-91-G-0047.

References and Notes

(1) Theodorou, D. N.; Suter, U. W. *Macromolecules* **1985**, *18*, 1467.
(2) Rigby, D.; Roe, R.-J. *J. Chem. Phys.* **1987**, *87*, 7285.
(3) Clarke, J. H. R.; Brown, D. *Mol. Simul.* **1989**, *3*, 27.
(4) Boyd, R. H. *Macromolecules* **1989**, *22*, 2477.
(5) Winkler, R. G.; Ludovice, P. J.; Yoon, D. Y.; Morawitz, H. *J. Chem. Phys.* **1991**, *95*, 4709.
(6) Li, Y.; Mattice, W. L. *Macromolecules* **1992**, *25*, 4942.
(7) Mark, J. E. *J. Am. Chem. Soc.* **1966**, *88*, 4354.
(8) Mark, J. E. *J. Am. Chem. Soc.* **1967**, *89*, 6829.
(9) Abe, Y.; Flory, P. J. *Macromolecules* **1971**, *4*, 219.
(10) Corradini, P.; Napolitano, R.; Petraccone, V.; Pirozzi, B.; Tuzi, A. *Eur. Polym. J.* **1981**, *17*, 1217.
(11) Corradini, P.; Napolitano, R.; Petraccone, V.; Pirozzi, B.; Tuzi, A. *Macromolecules* **1982**, *15*, 1207.
(12) Corradini, P.; De Rosa, C.; Zhi, G.; Napolitano, R.; Pirozzi, B. *Eur. Polym. J.* **1985**, *21*, 635.
(13) De Rosa, C.; Zhi, G.; Napolitano, R.; Pirozzi, B. *Macromolecules* **1985**, *18*, 2328.
(14) De Rosa, C.; Napolitano, R.; Pirozzi, B. *Polymer* **1985**, *26*, 2039.
(15) Molecular modeling software package, Molecular Simulations Inc.
(16) Dodge, R.; Mattice, W. L. *Macromolecules* **1991**, *24*, 2709.
(17) Zhan, Y.; Mattice, W. L. *Macromolecules* **1992**, *25*, 1554.
(18) Zhan, Y.; Mattice, W. L. *J. Chem. Phys.* **1992**, *96*, 3279.
(19) van Krevelen, D. R.; Hoftyzer, P. J. *Properties of Polymers-Their Estimation and Correlation with Chemical Structure*; Elsevier: New York, 1976; pp 130, 137, and 275.
(20) Lee, K.-J.; Mattice, W. L. *Comput. Polym. Sci.* **1992**, *2*, 55.
(21) Yoon, D. Y.; Sundararajan, P. R.; Flory, P. J. *Macromolecules* **1975**, *8*, 776.
(22) Flory, P. J. *Statistical Mechanics of Chain Molecules*; Hanser: New York, 1989, p 217.